Experimental Comparison of Single-Carrier and Digital Subcarrier Multiplexing Transmissions in a W-Band 200 Gb/s Fiber-Wireless System Considering Transmitter IQ Imbalance and Skew Mitigation

Weidong Tong, Jiao Zhang, Min Zhu, Xiang Liu, Yingxin Wei, Bingchang Hua, Zhigang Xin, Mingzheng Lei, Yuancheng Cai, Yucong Zou, Liang Tian, and Guo Zhao

***Abstract*—In fiber-wireless integration systems, it is valuable to investigate whether digital subcarrier multiplexing (SCM) signal is effective in improving nonlinear tolerance against photodiode (PD) saturation compared to single-carrier (SC) signal. For a fair comparison, the mitigation of linear impairments especially for IQ mixing effects become significant. In this article, we first analyze the impacts of transmitter IQ mixing effects for SC and digital SCM signals. Then, we employ the real-valued multiple-input multiple-output (MIMO) post-equalizers for the PM (polarization multiplexing)-SC system and PM-SCM system so as to mitigate transmitter IQ mixing effects. Finally, we experimentally compare the nonlinear tolerance of SC, SCM with two subcarriers (SCM-2), and SCM-4 signals using QPSK, 8QAM, and 16QAM in a W-band fiber-wireless system against the pin-photodiode (PIN-PD) saturation considering noise-limited case, optimum case and non-linear case. Subcarriers for SC, SCM-2, and SCM-4 are 25GBaud, 12.5GBaud, and 6.25GBaud respectively, with a total symbol rate of 25GBaud. Maximum line rate is 200 Gb/s with the BER satisfying the 7% HD-FEC threshold when employing the PM-16QAM. The results show that SCM signal has better nonlinear tolerance against the PIN-PD saturation than SC signals when system works in the non-linear case especially when using high-order modulation formats.**

***Index Terms*—Fiber-wireless system, digital subcarrier multiplexing, IQ mixing effects, nonlinear tolerance.**

Manuscript received 16 April 2023; revised 29 May 2023; accepted 11 June 2023. Date of publication 14 June 2023; date of current version 26 June 2023. This work was supported in part by the National Natural Science Foundation of China under Grants 62101121, 62101126, 62201397, 62201393, and 62271135, in part by the project funded by China Postdoctoral Science Foundation under Grant 2021M702501 and 2022T150486, in part by the State Key Laboratory of Advanced Optical Communication Systems and Networks of Shanghai Jiao Tong University through the open project under Grant 2022GZKF003, in part by the Major Key Project of Peng Cheng Laboratory under Grant PCL 2021A01-2, in part by the Key Research and Development Program of Jiangsu Province under Grant BE2020012, and in part by the Graduate Research and Innovation Projects of Jiangsu Province under Grant SJCX23_0038. *(Corresponding authors: Jiao Zhang; Min Zhu.)*

Weidong Tong, Jiao Zhang, Min Zhu, Xiang Liu, Yingxin Wei, Zhigang Xin, and Yuancheng Cai are with the National Mobile Communications Research Laboratory, Southeast University, Nanjing 210096, China, and also with Purple Mountain Laboratories, Nanjing 211111, China (e-mail: weidongtong@seu.edu.cn; jiaozhang@seu.edu.cn; minzhu@seu.edu.cn; xianglliu@seu.edu.cn; yingxinwei@seu.edu.cn; zhigangxin@seu.edu.cn; caiyuancheng@pmlabs.com.cn).

Bingchang Hua, Mingzheng Lei, Yucong Zou, and Liang Tian are with Purple Mountain Laboratories, Nanjing 211111, China (e-mail: huabingchang@pmlabs.com.cn; 2016010326@bupt.cn; zouyucong@pmlabs.com.cn; tianliang@pmlabs.com.cn).

Guo Zhao is with Science and Technology Management Department, Nanjing Wasin Fujikura Optical Communication LTD., Nanjing 210038, China (e-mail: guo_zhao@nwf.cn).

Digital Object Identifier 10.1109/JPHOT.2023.3286101

I. Introduction

THE fiber-wireless integrated networks leverage both fiber and wireless links to realize high-capacity and ubiquitous wireless access, effectively addressing challenges related to dimensioning, scalability, and quality of service (QoS) for users [1], [2]. Different with fiber nonlinearity in optical transmission systems, nonlinear effect induced by photodiode (PD) saturation becomes a limiting factor in fiber-wireless system. Digital subcarrier multiplexing (SCM) technology has attracted much attention among several researches. By splitting the high-baud rate single carrier (SC) signal into multiple multiplexed low-baud-rate subcarriers and optimizing the number of subcarriers, the nonlinearity tolerance of the system can be improved [3], [4], [5], [6]. The comprehensive set of experiments, simulations and analytical results on the benefit of nonlinear mitigation strategies for SCM polarization multiplexed 16 quadrature amplitude modulation (PM-16QAM) fiber transmission system is reported. However, the impacts of digital SCM technology are only investigated in optical fiber transmission systems [7]. The seamless full-duplex fiber-wireless system in the W-band for SCM signal transmission is reported in [8], but the nonlinear tolerance of digital SCM technology has not been investigated. In [9], the nonlinear tolerance of orthogonal frequency-division multiplexing (OFDM) and Nyquist-SCM signals against power amplifier (PA) saturation is only studied by simulated analysis. To the best of our knowledge, no research work has been reported on comparing the nonlinear tolerance against pin-photodiode (PIN-PD) saturation of the SC signal and SCM signal in the W-band fiber-wireless system.

Meanwhile, a higher symbol rate with higher-order modulation format is more susceptible to the in-phase (I) and quadrature (Q) imperfections in the transceiver caused by component defects or misalignments, such as gain imbalance, phase imbalance, and skew, which are referred to IQ mixing effects, could lead to significant degradation of system performance

[10], [11]. In order to fairly compare the nonlinear tolerance of SC and SCM signals in the large capacity fiber-wireless integration system, the mitigation of linear impairments such as IQ mixing effects becomes especially important. Therefore, the real-valued multiple-input multiple-output (MIMO) adaptive post-equalizers can be utilized to compensate for the IQ mixing effects in PM-SC and PM-SCM systems [12], [13].

In this article, we first analyze and prove that the impact of the transmitter IQ power/phase imbalance and IQ skew on PM-SC and PM-SCM signals can be effectively compensated by the real-valued MIMO post-equalizers. Then, we experimentally compare the nonlinear tolerance of PM-SCM signals and PM-SC signals in the W-band fiber-wireless system with different input optical power (IOP) into PIN-PD. Three kinds of modulation formats including QPSK, 8QAM, and 16QAM are employed in SC and SCM systems. The BER performance and polarization stability for SC and SCM systems are detailly analyzed. The maximum line rate is 200 Gb/s with the BER satisfying the 7% HD-FEC threshold. The EVM penalty between dual polarizations for 16QAM is smaller than 4% which shows the high polarization stability.

II. Analysis of Transmitter IQ Mixing Effects

A. Impact in SC System

In order to conduct a more accurate analysis and comparison of the nonlinear tolerance against PIN-PD saturation in SC and SCM signals, it is crucial to eliminate linear impairments such as IQ mixing effects and polarization crosstalk, which could have a negative impact on the comparison results. Among these linear impairments, Tx IQ mixing effects are particularly critical, as they can significantly deteriorate the performance of coherent communication systems. Therefore, it is essential to analyze and evaluate the impacts of Tx IQ mixing effects in SC and SCM systems. In this sub-section, we will first focus on the SC system. In general case, an IQ Mach-Zehnder modulators (MZM) operates in the linear region. Considering that a fiber-delay-based polarization-division multiplexing (PDM) emulator realizes dual polarization signals, so we need only one IQ modulator in the experiment as shown in Fig. 1. Therefore, we only consider the IQ mixing effects in a single polarization, and the IQ mixing effect between the two polarizations is not discussed here. The idea baseband SC signal before the IQ modulation is $S(t)$ which can be expressed as:

$$S(t) = S_I(t) + jS_Q(t) \tag{1}$$

where $S_I(t)$and $S_Q(t)$ are real and imaginary parts of the SC signal, respectively. However, in real devices, the I and Q branches are not perfectly balanced and synchronized. The presence of such imperfections can lead to the occurrence of I/Q mixing which causes severe degradation of system performance. After passing through the IQ modulator, the output signal of Tx can be expressed as:

$$\begin{aligned} S_{Tx}(t) &\propto [S_I(t) + p \cdot S_Q(t+\triangle\tau)\exp(j(\pi/2+\varphi))] \\ &= [S_I(t) - p \cdot S_Q(t+\triangle\tau)\sin(\varphi) + jp \cdot S_Q(t+\triangle\tau)\cos(\varphi)] \end{aligned}$$

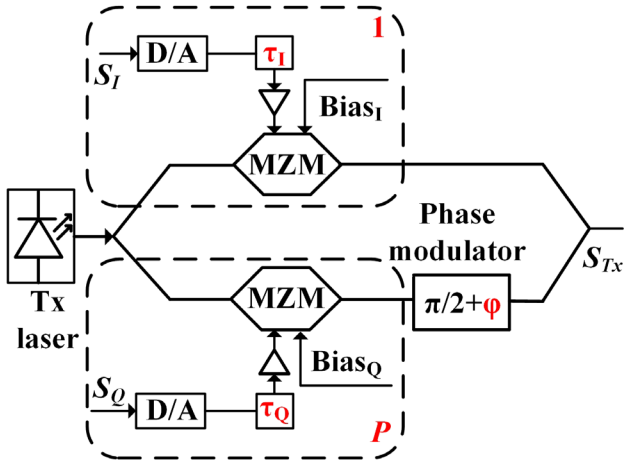

Fig. 1. IQ modulator with Tx IQ mixing effects including IQ power imbalance, IQ phase imbalance and IQ skew.

$$= \hat{S}_I(t) + j\hat{S}_Q(t) \tag{2}$$

which could be rewritten by the matrix equation:

$$\begin{pmatrix} S'_I(t) \\ S'_Q(t) \end{pmatrix} = \begin{pmatrix} 1 & -p\sin\varphi \\ 0 & p\cos\varphi \end{pmatrix} \begin{pmatrix} 1 & 0 \\ 0 & \delta(t+\triangle\tau) \end{pmatrix} \begin{pmatrix} S_I(t) \\ S_Q(t) \end{pmatrix} \tag{3}$$

The component of channel I is preset to the ideal signal given that the IQ mixing effects is the relative value of the I and Q channel. For simplification, we assume the component of channel I with a magnitude of 1 and a phase shift of 0. Therefore, $P$and φ represent the IQ power imbalance and IQ phase imbalance parameters of Tx, respectively. In addition, $\delta_{dB} = 20\log_{10}p$ used to define the IQ power imbalance in dB. $\Delta\tau$ equals to $\tau_Q - \tau_I$ which is the parameter of IQ skew. Obviously, (3) is a linear transformation which means that IQ mixing effects can be fully compensated by the 2×2 real-valued MIMO equalizer for single polarization signal. However, for the dual polarization (DP) signal, considering that the potential crosstalk between two polarizations, 4×4 real-valued MIMO equalizer [12] is a better choice to maintain system performance which is given by:

$$\begin{bmatrix} X_I \\ X_Q \\ Y_I \\ Y_Q \end{bmatrix} = \begin{bmatrix} f_{1,1[n]} & f_{1,2[n]} & f_{1,3[n]} & f_{1,4[n]} \\ f_{2,1[n]} & f_{2,2[n]} & f_{2,3[n]} & f_{2,4[n]} \\ f_{3,1[n]} & f_{3,2[n]} & f_{3,3[n]} & f_{3,4[n]} \\ f_{4,1[n]} & f_{4,2[n]} & f_{4,3[n]} & f_{4,4[n]} \end{bmatrix} \begin{bmatrix} x_I \\ x_Q \\ y_I \\ y_Q \end{bmatrix} \tag{4}$$

where the inputs are the real and imaginary parts of the complex-valued polarization multiplexing signals(x, y) $x_I = \mathrm{Re}(x), x_Q = \mathrm{Im}(x), y_I = \mathrm{Re}(y), y_Q = \mathrm{Im}(y)$.Let$f_{i,j}[n]$ be the real impulse response of the digital filter from the $i-$th input to the $j-$th output of the equalizer, where $i, j \in \{1, \ldots, 4\}$and $n \in \{0, \ldots, M-1\}$with M being the number of taps of the filters. Therefore the 4×4 real-valued MIMO equalizer including 16 filters with M taps each.

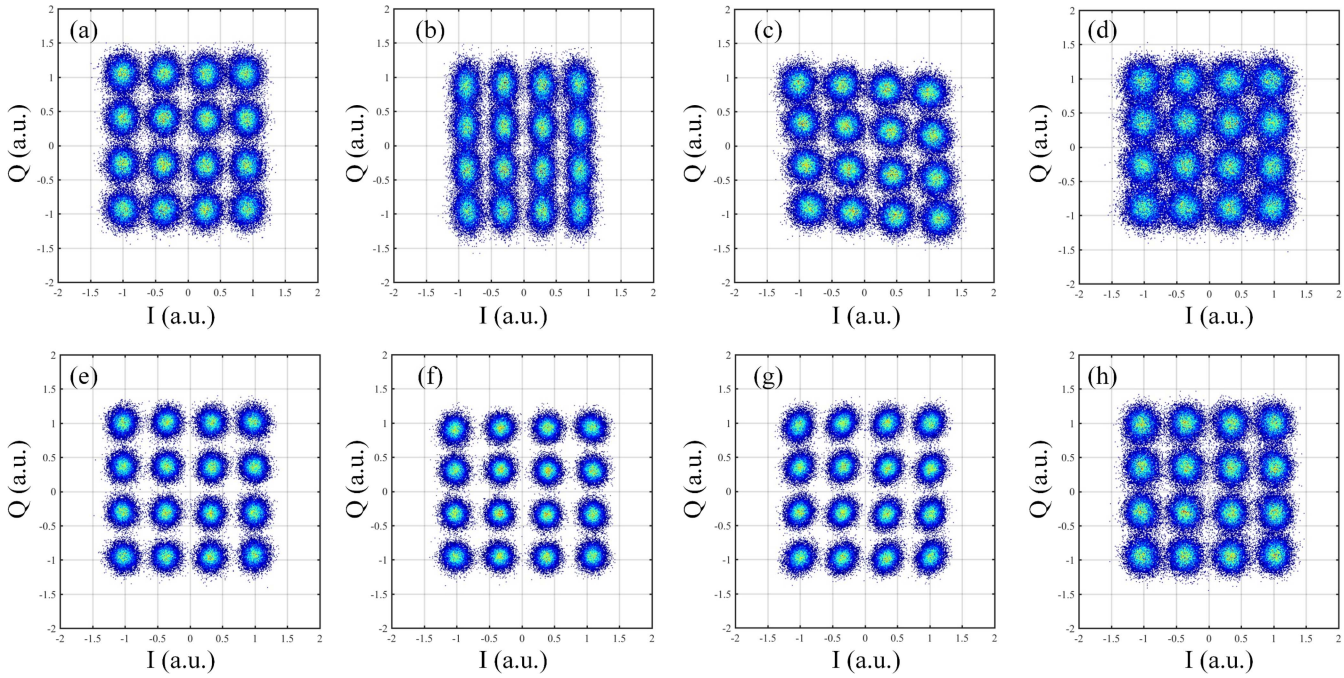

Fig. 2. (a) Received 16QAM SC signal constellation without IQ mixing; (b) with 2.5 dB IQ power imbalance; (c) with 10-degree IQ phase imbalance; (d) with 4 ps IQ skew; employ 4 × 4 real-valued MIMO post-equalization: (e) Received 16QAM constellation without IQ mixing; (f) with 2.5 dB IQ power imbalance; (g) with 10-degree IQ phase imbalance; (h) with 4 ps IQ skew.

Since it was not possible to set a precise and wide range of IQ skew and IQ imbalance values by changing the hardware parameters at the transmitter side. To add a specific value, IQ mixing effects are added to the original signal by the transmitter DSP according to (2). The experimental setup is described in detail in Section III. Next, the impact of Tx IQ mixing effects on the signal constellation is discussed. The received 16QAM signal constellation without IQ mixing effects is shown in Fig. 2(a). The 16QAM signal constellation with 2.5 dB IQ power imbalance is shown in Fig. 2(b). We can observe that the four clusters of symbols in the Q direction are connected together due to the IQ power imbalance. Fig. 2(c) depicts the 16QAM signal constellation with 10-degree IQ phase imbalance. The constellation distortion from square to parallelogram can be found. Fig. 2(d) shows the 16QAM signal constellation with 4 ps IQ skew. We can note that neighboring clusters are closer together, which means that symbol decision is more difficult according to the standard constellation. The effectiveness of the post-equalizer can be proved by the improvement of the constellation quality. Then, Fig. 2(e)–(h) show the 16QAM signal constellation after the 4 × 4 real-valued MIMO post-equalization. Note that Fig. 2(e)–(h) correspond to Fig. 2(a)–(d), respectively. Fig. 2(e) shows a clearer distribution of constellation points compared to Fig. 2(a), which means that even without the IQ mixing effects, the equalizer improves system performance by eliminating impairments such as polarization crosstalk. The performance of a real-valued MIMO post-equalizer depends on relevant parameters such as the number of filter taps, update step size, and the number of training symbols, which have been adjusted to appropriate values. As can be seen in Fig. 2(f)–(h), the constellation with post-equalizer is better than the corresponding one without post-equalizer.

B. *Impact in SCM System*

For simplicity, we analyze a SCM system with two frequency-symmetric subcarriers, but an identical analysis applies to a general SCM system with any number of subcarriers. As in the previous analysis of SC signals, we consider for simplicity a single polarization, but an identical analysis could be performed on the other polarization. Fig. 3(a) shows the 25 GBaud SCM-2 signal spectrum without IQ mixing effects in the transmission side. To intuitively demonstrate the impact of IQ mixing effects on the spectrum of SCM signal, subcarrier-1's spectra of the SCM signal is shown separately in Fig. 2(b). Then, the spectrum when IQ mixing effects exist is depicted in Fig. 3(c). It can be observed that interference occurs at a symmetrical position of the subcarrier-1 spectrum, precisely where subcarrier 2 is located. The spectrum with 3 dB IQ power imbalance as shown in Fig. 3(d). Similar to the effects of IQ power imbalance, Fig. 3(e) shows the spectrum with 10-degree IQ phase imbalance. Fig. 3(f) depicts the spectrum with 10 ps IQ skew. Specifically, the higher the frequency, the more severe the interference at its symmetrical position. Generalizing to more general cases, it is evident that in the presence of IQ mixing effects, interference occurs between each pair of subcarriers symmetrically in the frequency domain of SCM signals. Next, we will prove it by mathematical derivation. The baseband subcarriers are defined as $m_1(t)$and $m_2(t)$, respectively. They can be expressed as:

$$m_1(t) = I_1(t) + jQ_1(t) \qquad m_2(t) = I_2(t) + jQ_2(t) \quad (5)$$

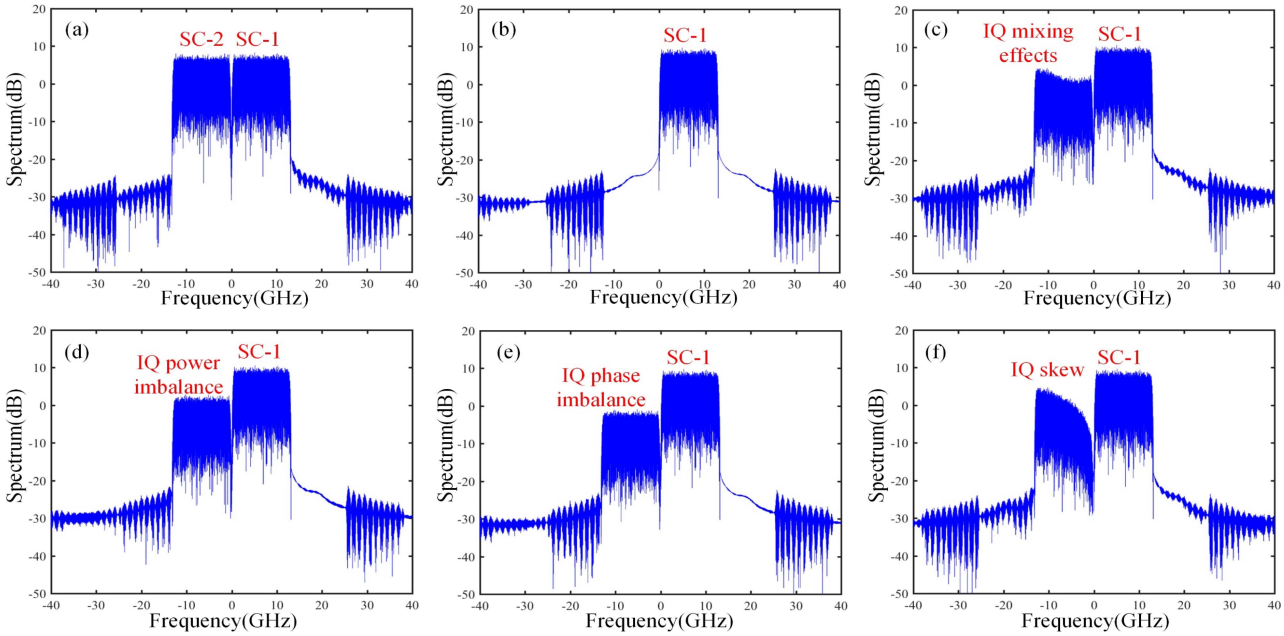

Fig. 3. (a) Tx 25 GBaud SCM-2 signal spectrum without IQ mixing; positive half of the Tx 25GBaud SCM-2 signal spectrum (b) without IQ mixing; (c) with IQ mixing including 3 dB IQ power imbalance, 10-degree IQ phase imbalance and 10 ps IQ skew; (d) with 3 dB IQ power imbalance; (e) with 10-degeree IQ phase imbalance; (f) with 10 ps IQ skew.

The center angular frequencies of the two subcarriers are w_n and $-w_n$, respectively. After frequency shift, we rename these two subcarriers as $s^+(t)$and $s^-(t)$, respectively. They can be written in terms of the baseband in-phase and quadrature components as:

$$\begin{aligned} s^+(t) &= [I_1(t) + jQ_1(t)]e^{jw_n t} \\ s^-(t) &= [I_2(t) + jQ_2(t)]e^{-jw_n t} \end{aligned} \tag{6}$$

Therefore, the SCM signal $s^{\pm}(t)$ can be expressed as:

$$s^{\pm}(t) = s^+(t) + s^-(t) = I^{\pm}(t) + jQ^{\pm}(t) \tag{7}$$

where $I^{\pm}(t)$and $Q^{\pm}(t)$ are real and imaginary parts of the SCM signal, respectively. They can be represented as:

$$\begin{aligned} I^{\pm}(t) &= [I_1(t) + I_2(t)]\cos w_n t + [Q_2(t) - Q_1(t)]\sin w_n t \\ Q^{\pm}(t) &= [I_1(t) - I_2(t)]\sin w_n t + [Q_2(t) + Q_1(t)]\cos w_n t \end{aligned} \tag{8}$$

Similar with the SC signal, g, θ and τ denote the power imbalance, phase imbalance and skew parameters of Tx, respectively. After passing through the IQ modulator, the generated signal $\hat{s}^{\pm}(t)$ can be written as:

$$\hat{s}^{\pm}(t) = I^{\pm}(t) + jg \cdot Q^{\pm}(t+\tau)e^{j\theta} = \hat{I}^{\pm}(t) + j\hat{Q}^{\pm}(t) \tag{9}$$

Note that each subcarrier of the SCM signal is frequency shifted from the baseband signal compared to the SC signal. After the receiver DSP, the received two baseband signals can be expressed as:

$$\begin{aligned} r_1(t) &= LPF\left\{\hat{s}^{\pm}(t) \cdot e^{-jw_n t}\right\} \\ r_2(t) &= LPF\left\{\hat{s}^{\pm}(t) \cdot e^{jw_n t}\right\} \end{aligned} \tag{10}$$

which could be expressed in the form of matrix:

$$\begin{aligned} \begin{pmatrix} I_{r_1}(t) \\ Q_{r_1}(t) \\ I_{r_2}(t) \\ Q_{r_2}(t) \end{pmatrix} &\propto \frac{1}{2} \times M \times \begin{pmatrix} I_1(t) \\ Q_1(t) \\ I_2(t) \\ Q_2(t) \end{pmatrix} + \frac{1}{2} \times H \\ &\times \begin{pmatrix} I_1(t+\tau) \\ Q_1(t+\tau) \\ I_2(t+\tau) \\ Q_2(t+\tau) \end{pmatrix} \end{aligned} \tag{11}$$

while all 16 elements in *M* are constant values, the 16 elements in *H* depend on four variables that are determined by the parameters of IQ mixing effects. Both *M* and *H* are 4×4 matrices, which can be expressed in detail as follows:

$$\begin{aligned} M &= \begin{pmatrix} 1 & 0 & 1 & 0 \\ 0 & 1 & 0 & -1 \\ 1 & 0 & 1 & 0 \\ 0 & -1 & 0 & 1 \end{pmatrix} \\ H &= \begin{pmatrix} h_{11} & -h_{21} & -h_{11} & -h_{21} \\ h_{21} & h_{11} & -h_{21} & h_{11} \\ h_{31} & h_{41} & -h_{31} & h_{41} \\ h_{41} & -h_{31} & -h_{41} & -h_{31} \end{pmatrix} \end{aligned} \tag{12}$$

where the h_{i1} ($i \in \{1, \ldots, 4\}$) refer to the specific values:

$$\begin{aligned} h_{11} &= g\cos(w_n\tau + \theta) & h_{21} &= g\sin(w_n\tau + \theta) \\ h_{31} &= -g\cos(w_n\tau - \theta) & h_{41} &= g\sin(w_n\tau - \theta) \end{aligned} \tag{13}$$

In fact, (11) indicates that the signals coming from the symmetric SC at angular frequency w_n have to be jointly processed with the components of the SC at angular frequency $-w_n$ to completely eliminate interference. In addition, we find that (11)

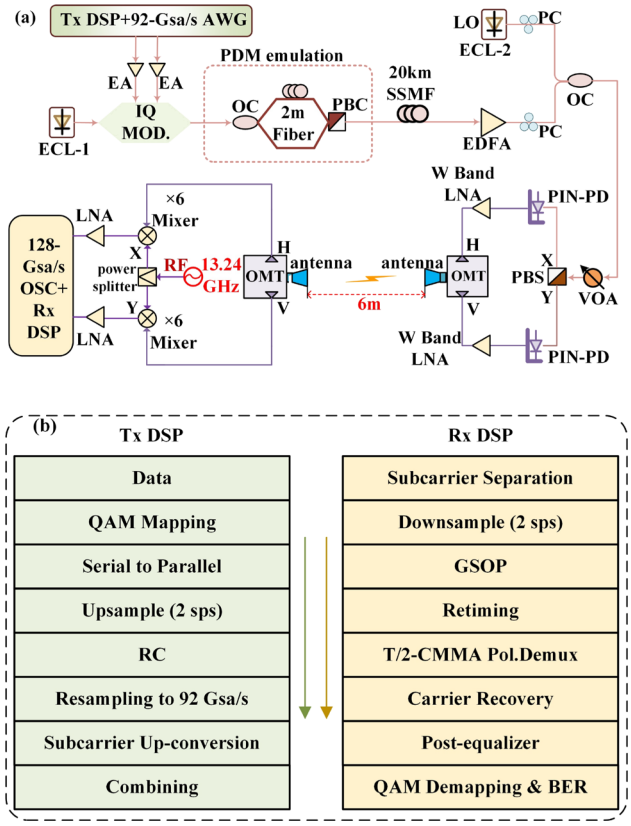

Fig. 4. (a) Experimental setup of W-band PM wireless transmission system; (b) Tx and Rx off-line DSP blocks.

is a linear transformation which means that IQ mixing effects can be fully compensated by the 4 × 4 real-valued MIMO equalizer. As for the dual-polarization signal, we employ the 8 × 8 real-valued MIMO equalizer [13] to maintain system performance. Each polarization of the two frequency-domain symmetric subcarriers has two components, resulting in a total of eight real-valued components. The structure of 8 × 8 real-valued MIMO equalizer is similar with the 4 × 4 real-valued MIMO equalizer. Both two post-equalizers are updated through a standard decision-directed least mean square (DD-LMS) algorithm. The detailed analysis of the MIMO equalization algorithm is not a priority and is therefore not discussed in the article.

III. Experimental Setup

We experimentally compared the nonlinear tolerance against PIN-PD saturation in SC and SCM signals for 200 Gb/s fiber-wireless system at W-Band. The experimental setup of the W-band PM wireless transmission system is illustrated in Fig. 4(a). One free-running tunable external cavity laser (ECL-1) with 100 kHz linewidth operating at 193.4075 THz is used as the optical input of a 35 GHz I/Q modulator. The electrical baseband signal is generated from a 92 Gsa/s AWG with 3 dB analog bandwidth of 32 GHz and 8-bit resolution. The I/Q modulator is biased at a null point and driven by two 40 GHz electrical amplifiers (EA). A fiber-delay-based PDM emulator realizes polarization-division multiplexing (PDM) with 2 m of decorrelation delay. After transmitting the 20 km standard single-mode fiber (SSMF), the baseband optical signals are boosted by an EDFA. The optical signals and the local oscillator (LO) operating at 193.5 THz are coupled and then controlled by a variable optical attenuator (VOA) to set the value of IOP into PIN-PDs effectively. Fig. 5(a) shows the spectrum of the optical modulated signal and LO signal, indicating a frequency spacing of 92.5 GHz between the two signals. The dual polarization is achieved through a polarization beam splitter (PBS) and then up-converted by PIN-PDs to W-band 92.5GHz wireless signals. To balance the optical power into the two polarization-sensitive PIN-PDs, two polarization controllers (PCs) are required to adjust the incident polarization state. Following the W-band low noise amplifier (LNA), the ortho-mode transducer (OMT) couples the X and Y polarizations into the circularly polarized antenna. Compared with the traditional structure of the wireless link, only a pair of antennas is employed in our system thanks to the OMTs.

Then the W-band 92.5GHz signals from the antenna are delivered over a 6 m wireless link. The W-band transmitter and receiver are placed at the height of 1m to avoid multi-path fading from reflections on the ground. The W-band receiver is driven by an electronic LO source to implement analog down conversion, and has a mixer with ×6 frequency multiplier chain for each polarization of the received signals. The LO source is set to be 13.24 GHz, corresponding to the intermediate frequency (IF) signals of 13.06 GHz. Finally, after the amplification of the low-noise amplifier (LNA), the X-polarization and Y-polarization IF signals are captured by the real-time oscilloscope (OSC). The spectra of the received signals for SC, SCM-2, and SCM-4 belonging to the X polarization are shown in Fig. 5(b). The raised-cosine (RC) pulse shaping technique with a 5% rolloff factor is utilized, which corresponds to the subcarrier bandwidths of 26.25GHz, 13.125GHz, and 6.5625GHz for the SC, SCM-2, and SCM-4 systems, respectively. Note that the mentioned subcarrier bandwidths are approximate values for the real case. The actual bandwidths can be quite intricate to describe as they need to fulfill the requirement of maximizing the input symbol length in the AWG.

Fig. 4(b) demonstrates the Tx and Rx offline DSP blocks for SCM signals. At Tx DSP, after serial to parallel conversion, data corresponding to different subcarriers was independently mapped to a specific modulation format. In this experiment, we kept the aggregate symbol rate to 25 GBaud. The mapped symbols were up sampled by a factor of 2, and a raised-cosine (RC) pulse shaping filter with a roll-off factor of 0.05 was applied. The shaped digital subcarriers were resampled to match DACs sampling frequency of 92 Gsa/s and then shifted in frequency and summed up, resulting in a SCM signal. Note that there was no guard band between subcarriers, so the total bandwidth of the signal is 26.25 GBaud. At receiver DSP, since each subcarrier can be independently processed after down-conversion to baseband and low-pass filter (LPF), the same DSP algorithms work for both SC and SCM signals. Then resampling was applied to get 2 Samples/symbol streams for each subcarrier. Steps of gram-schmidt orthogonalization procedure (GSOP), timing recovery, 2 × 2 blind equalizer adaptation using cascaded multi-modulus algorithm (CMMA), frequency offset compensation,

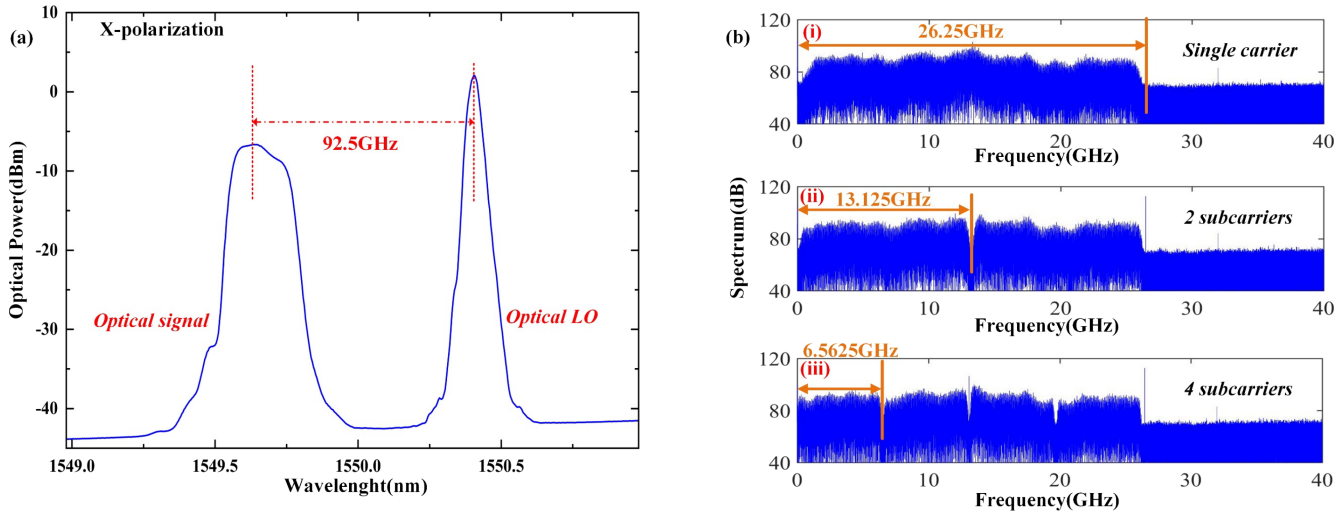

Fig. 5. (a) The spectrums of optical modulated signal and local oscillator (LO) signal belongs to X-polarization; (b) the spectrum of received 16QAM X-polarization signals for (i) SC (ii) SCM-2 (iii) SCM-4 system.

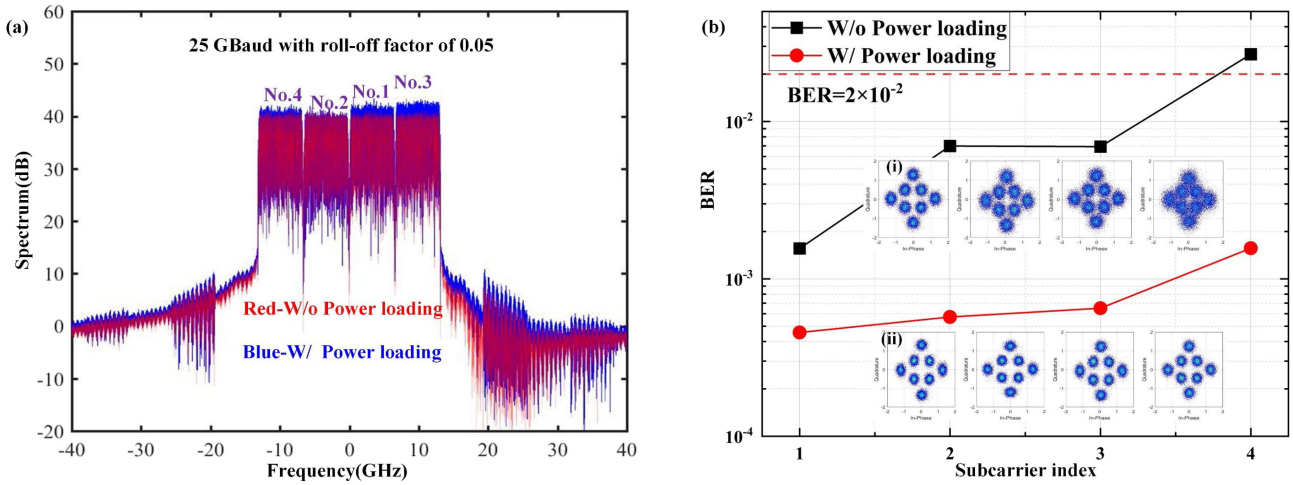

Fig. 6. (a) The Spectrum of SCM-4 Tx signal with power loading and without; (f) the BER performance of different subcarriers for SCM-4 8QAM signals without MIMO post -equalization when IOP is 3dBm and the corresponding constellation diagrams in inset (i), (ii).

and phase recovery using blind phase search (BPS) followed. Finally, we employ the MIMO post-equalizers to further improve the system performance. Considering that the channel response of 4 subcarriers for SCM-4 signal is not flat, we implement power loading to the SCM-4 signal by calculating the SNR at the receiver and choose an appropriate weighting factor for each subcarrier which is shown in Fig. 6(a). The red spectrum is the original signal without power loading and the blue spectrum is the signal with power loading. It is worth noting that the signal undergoes energy normalization before being fed into the AWG to ensure a constant total symbol energy. We then pick out the X- polarization of SCM-4 signals with 8QAM modulation when the IOP is set to 3 dBm. To emphasize the impact of power loading technology on system performance, Fig. 6(b) shows the BER performance of each subcarrier for SCM-4 system without utilizing the MIMO post-equalization. Power loading helps mitigate the impact of interference by allocating lower power to subcarriers with poor channel conditions. Conversely, higher power can be allocated to subcarriers experiencing severe fading to enhance received signal quality. This strengthens the system's resilience to interference and fading, improving communication quality and reliability. The constellations of the signals without and with power loading are shown as inset (i) and inset (ii), respectively, which proves the effectiveness of power loading to equalize each subcarrier.

IV. Results and Discussion

To compare the nonlinear tolerance induced by PIN-PD saturation of SC and SCM systems, we measured the mean BER versus input optical power into PIN-PD for QPSK, 8QAM and 16QAM signals, respectively. The BER is the average value of

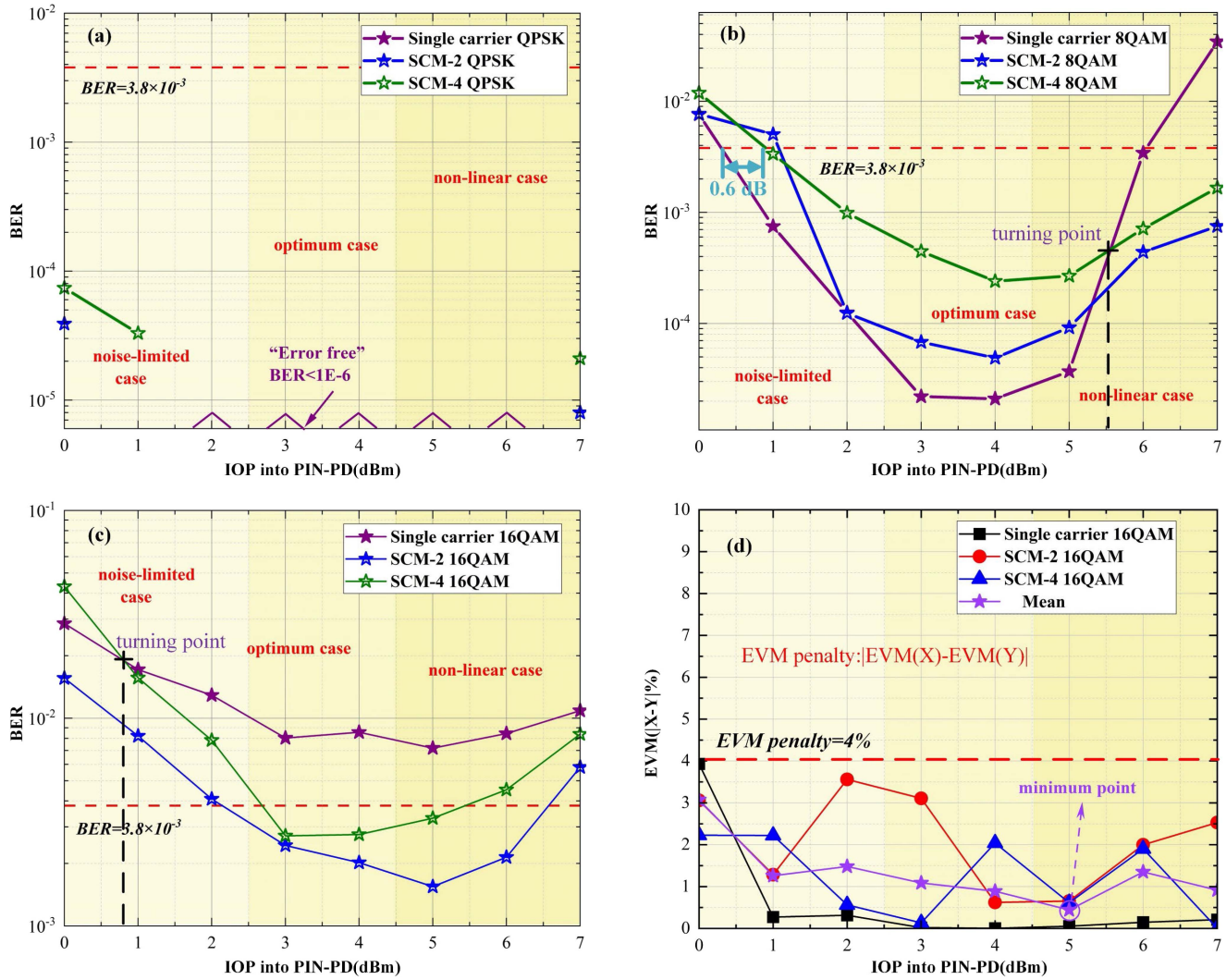

Fig. 7. Comparison of BER performance of SC, SCM-2 and SCM-4 systems versus IOP into PIN-PDs for (a) QPSK (b) 8QAM (c) 16QAM signals; (d) the EVM penalty between two polarizations of SC, SCM-2 and SCM-4 systems versus IOP into PIN-PDs.

all subcarriers of X and Y polarization. We applied the principles outlined in [14] for partitioning the operating region of the PIN-PD to our experimental system. Note that the behavior of the BER curves is non-monotonic. Initially, the performance of the system improves as the IOP increases (and so the signal-to-noise ratio). However, beyond certain value of IOP, the BER performance starts to degrade. This effect can be attributed to non-linear behavior induced by PIN-PD saturation effect. To ensure uniform partitioning and facilitate intuitive demonstration of system performance across the three modulation formats, we categorized the operating region of the PIN-PD into three cases based on the BER of the 8QAM system. When the IOP is between 0 and 2.5 dBm, the Pin-PD works in the noise-limited case. The optimum case is between 2.5 and 4.5 dBm, and the nonlinear case is between 4.5 and 7 dBm. For the QPSK signals, as shown in Fig. 7(a), the BER of SC, SCM-2 and SCM-4 signals are all below the threshold of 3.8×10^{-3}. Although the SC signal performs slightly better than the two kinds SCM signals in the IOP of 0, 1 and 7 dBm, error-free transmission is achieved in the majority of IOP for SCM-2 and SCM-4 systems. Excellent system performance is realized at the expense of spectrum efficiency for the QPSK signals. As shown in Fig. 7(b) for 8QAM, considering the 7% HD-FEC threshold at 3.8×10^{-3}, 4 dBm is the minimum point for SC, SCM-2 and SCM-4 signals. Compared with the SC signal, the SCM-4 signal has brought 0.6 dB while the SCM-2 signals has brought 0.8 dB sensitivity penalty in the noise-limited case. 5.6 dBm is the turning point for 8QAM signals, which means that the SCM systems perform better than the SC system when the IOP exceeds 5.6 dBm. The reason for the severe degradation of BER performance in SCM-2 system at an IOP of 1dBm, which is even worse than that of SCM-4 system, is due to polarization state drift. Specifically, the polarization state of optical signals may be influenced by environmental factors, fiber characteristics, or imperfections in devices, among other factors. This drift can result in unequal output power of polarization state signals, impacting the quality and transmission performance of the signals. In addition, we note that the SC system performance deteriorates dramatically

in the nonlinear region while the BER curves of SCM-2 and SCM-4 systems are still below the HD-FEC threshold.

For the 16QAM signals shown in Fig. 7(c), the minimum BER for both SC and SCM-2 systems occurs when the IOP is 5 dBm. In the range of 0 dBm to 7 dBm, the SC system is unable to meet the HD-FEC threshold regardless of the IOP. However, this is not the case for the SCM systems. The IOP that meets the threshold ranges from 2.1 dBm to 6.6 dBm for SCM-2 system and 2.7 dBm to 5.5 dBm for SCM-4 system. When employing 16QAM, the digital SCM systems demonstrate a higher tolerance to nonlinear effects compared to the SC system. Besides, we note that the BER performance of SCM-2 signals is better than SCM-4 signals, which shows the importance of symbol rate optimization (SRO) in practical system. Digital SCM technology achieves SRO by dividing a high-speed data stream into appropriate number of multiple subcarriers and transmitting them in parallel over different subcarriers. This approach reduces the symbol rate and bandwidth requirements for each subcarrier, allowing efficient utilization of the channel bandwidth. Additionally, the technology compensates for frequency-selective fading and performs equalization on each subcarrier, minimizing the impact on transmission quality. Therefore, it is crucial to select an appropriate number of subcarriers for multiplexing based on the channel characteristics of the specific system. It is worth noting that the turning point for QPSK is more likely to be over 7 dBm from Fig. 7(a). 5.6 dBm is the turning point for 8QAM while 0.8 dBm is the turning point for 16QAM to distinguish the performance of SCM signals and SC signals. Therefore, we conclude that as the modulation order increases, the value of the turning point decreases, which means the nonlinear tolerance of SC signals deteriorates faster than digital SCM signals in high spectrum efficiency. Finally, considering that the results are in terms of the mean BER of the X polarization and Y polarization, we need to ensure that the performance of the two polarization is similar to support the reliability of the experimental results. In addition, the performance differences between two polarizations are worthy of attention. As shown in Fig. 7(d), 5 dBm is the minimum point of the mean value. The EVM of the penalty between two polarizations for 16QAM is smaller than 4% in all cases, which means the high stability of the performance of the two polarizations in the system. Hence, it is reliable to compare the SC and SCM systems based on the average BER of two polarizations.

V. Conclusion

We experimentally demonstrated a PM fiber-wireless system at W-Band using OMT. The aggregate symbol rate is 25 GBaud and the maximum rate is 200 Gb/s with the BER satisfying the 7% HD-FEC threshold. We investigated the mathematical model of transmitter IQ mixing effects including IQ power imbalance, phase imbalance, and skew on SC and SCM signals. We successfully verified that the impacts of transmitter IQ mixing effects on SC and SCM signals can be fully mitigated by the 4×4 and 8×8 real-valued MIMO equalizers in SC and SCM systems, respectively. Thanks to the MIMO equalizers, we effectively eliminate the effects of linear impairments especially for IQ mixing effects in order to fairly compare the nonlinear tolerance against the PIN-PD saturation of SC, SCM-2 and SCM-4 signals employing QPSK, 8QAM and 16QAM. The experimental results show that the SCM signal has better nonlinear tolerance against the PIN-PD saturation when employing the high order modulation, which can be meaningful for the large-capacity fiber-wireless system using digital SCM technology.

References

[1] S. Yao et al., "Data efficient estimation for quality of transmission through active learning in fiber-wireless integrated network," *J. Lightw. Technol.*, vol. 39, no. 18, pp. 5691–5698, Sep. 2021.

[2] J. Zhang et al., "Real-time demonstration of 100 GbE THz-wireless and fiber seamless integration networks," *J. Lightw. Technol.*, vol. 41, no. 4, pp. 1129–1138, Feb. 2023.

[3] M. Qiu et al., "Digital subcarrier multiplexing for fiber nonlinearity mitigation in coherent optical communication systems," *Opt. Exp.*, vol. 22, no. 15, pp. 18770–18777, 2014.

[4] M. Qiu et al., "Subcarrier multiplexing using DACs for fiber nonlinearity mitigation in coherent optical communication systems," in *Proc. Opt. Fiber Conf.*, 2014, Paper Tu3J.2.

[5] H. Nakashima, T. Tanimura, T. Oyama, Y. Akiyama, T. Hoshida, and J. C. Rasmussen, "Experimental investigation on nonlinear tolerance of subcarrier multiplexed signals with spectrum optimization," in *Proc. Eur. Conf. Opt. Commun.*, 2015, pp. 1–3.

[6] P. Poggiolini et al., "Analytical and experimental results on system maximum reach increase through symbol rate optimization," *J. Lightw. Technol.*, vol. 34, no. 8, pp. 1872–1885, Apr. 2016.

[7] F. P. Guiomar et al., "Nonlinear mitigation on subcarrier-multiplexed PM-16QAM optical systems," *Opt. Exp.*, vol. 25, no. 4, pp. 4298–4311, 2017.

[8] P. T. Dat et al., "Full-duplex transmission of Nyquist-SCM signal over a seamless bidirectional fiber–wireless system in W-band," in *Proc. Opt. Fiber Conf.*, 2019, Paper W1I.5.

[9] N. V. Dien et al., "Tolerance of SCM Nyquist and OFDM signals for heterogeneous fiber-optic and millimeter-wave mobile backhaul links under the effect of power amplifier saturation induced clipping," *Comput. Netw.*, vol. 204, 2022, Art. no. 108697.

[10] L. Dai et al., "Experimental demonstration of simultaneously precise Tx and Rx skew calibration for coherent optical transceiver," *J. Lightw. Technol.*, vol. 40, no. 4, pp. 1043–1054, Feb. 2022.

[11] M. Sato, M. Arikawa, H. Noguchi, J. Matsui, J. Abe, and E. L. T. de Gabory, "Transceiver impairment mitigation by 8×2 widely linear MIMO equalizer with independent complex filtering on IQ signals," *IEEE Photon. J.*, vol. 14, no. 3, Jun. 2022, Art. no. 7130911.

[12] E. P. da Silva and D. Zibar, "Widely linear equalization for IQ imbalance and skew compensation in optical coherent receivers," *J. Lightw. Technol.*, vol. 34, no. 15, pp. 3577–3586, Aug. 2016.

[13] G. Bosco et al., "Impact of the transmitter IQ-skew in multi-subcarrier coherent optical systems," in *Proc. Opt. Fiber Conf.*, 2016, Paper W4A.5.

[14] C. Castro et al., "32 GBd 16QAM wireless transmission in the 300 GHz band using a PIN diode for THz upconversion," in *Proc. Opt. Fiber Conf.*, 2019, Paper M4F.5.